SANDIA REPORT

SAND2017-13271
Unlimited Release
Printed October 2017

The use of multiwavelets for uncertainty estimation in seismic surface wave dispersion

Christian Poppeliers

Prepared by
Sandia National Laboratories
Albuquerque, New Mexico 87185 and Livermore, California 94550

Sandia National Laboratories is a multimission laboratory managed and operated by National Technology and Engineering Solutions of Sandia, LLC., a wholly owned subsidiary of Honeywell International, Inc., for the U.S. Department of Energy's National Nuclear Security Administration under contract DE-NA0003525.

Sandia National Laboratories

Issued by Sandia National Laboratories, operated for the United States Department of Energy by National Technology and Engineering Solutions of Sandia, LLC.

SAND2017-13271
Unlimited Release
Printed October 2017

The use of multiwavelets for uncertainty estimation in seismic surface wave dispersion

Christian Poppeliers
Geophysics Department
Sandia National Laboratories
P.O. Box 5800
Albuquerque, NM 87185-9999
cpoppel@sandia.gov

Abstract

This report describes a new single-station analysis method to estimate the dispersion and uncertainty of seismic surface waves using the multiwavelet transform. Typically, when estimating the dispersion of a surface wave using only a single seismic station, the seismogram is decomposed into a series of narrow-band realizations using a bank of narrow-band filters. By then enveloping and normalizing the filtered seismograms and identifying the maximum power as a function of frequency, the group velocity can be estimated if the source-receiver distance is known. However, using the filter bank method, there is no robust way to estimate uncertainty. In this report, I introduce a new method of estimating the group velocity that includes an estimate of uncertainty. The method is similar to the conventional filter bank method, but uses a class of functions, called Slepian wavelets, to compute a series of wavelet transforms of the data. Each wavelet transform is mathematically similar to a filter bank, however, the time-frequency tradeoff is optimized. By taking multiple wavelet transforms, I form a population of dispersion estimates from which standard statistical methods can be used to estimate uncertainty. I demonstrate the utility of this new method by applying it to synthetic data as well as ambient-noise surface-wave cross-correlelograms recorded by the University of Nevada Seismic Network.

Acknowledgment

The author acknowledges the National Nuclear Security Administration, Defense Nuclear Nonproliferation Research and Development (DNN RD), and the Source Physics Experiment (SPE) working group, a multi-institutional and interdisciplinary group of scientists and engineers. Sandia National Laboratories is a multimission laboratory managed and operated by National Technology and Engineering Solutions of Sandia LLC, a wholly owned subsidiary of Honeywell International Inc. for the U.S. Department of Energy's National Nuclear Security Administration under contract DE-NA0003525.

Contents

List of Figures

Chapter 1

Introduction

Seismic surface waves propagate along the air-solid interface of the Earth. Because the sensitivity kernels of surface waves is frequency dependent, longer wavelength surface waves tend to possess higher group and phase velocity due to the general increase of shear wave velocity with depth. By quantifying the propagation velocities of band limited surface waves, it is possible to gain an estimate of average shear-wave velocity structure of the Earth as a function of depth.

To estimate the dispersion of surface waves using only a single seismic station, one typically applies a series of narrow-band filters to a surface wave seismogram. The resulting suite of filtered seismograms are then enveloped, normalized and plotted as a function of time and frequency (Figure 1). By knowing the distance between the seismic source and the observing station, the resulting dispersion curve is transformed into slowness as a function of frequency (or period).

The maximum power of the surface wave at a given point in time and frequency will define the group velocity. However, this measurement gives no quantifiable estimation of uncertainty. To remedy this, I developed and describe a new method to estimate uncertainty of single-station dispersion curves which translate directly to uncertainties in the estimates of group- and phase-velocity of the surface waves. The method uses a class of orthogonal wavelet functions, known as Slepian wavelets, to decompose the seismogram into a series of mutually orthogonal time-frequency decompositions of a given signal. Each statistically independent wavelet transform can then be used to form a (statically independent) dispersion curve. I then apply standard statistical methods to estimate mean group- and phase-velocities of surface waves, as well as their uncertainties. I show the utility of the method by applying it to synthetic data as well as a series of surface wave cross correlograms collected by the University of Nevada Seismic network. Finally, I demonstrate how the uncertainty can be applied to 1D seismic tomography.

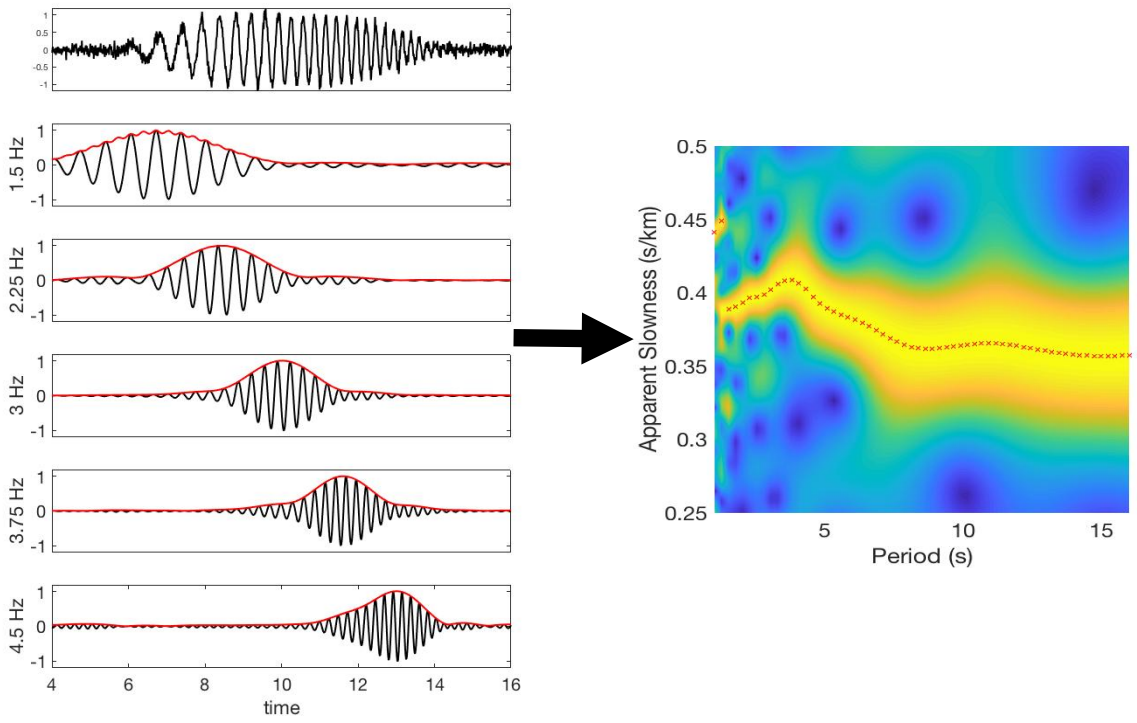

Figure 1.1. A synthetic example of using a bank of filters to estimate the dispersion of surface waves. The top panel on the left show a synthetic, dispersive seismogram. The panels immediately below that show the results of applying a series of narrow band filters to the original seismogram. The red line shows the envelope of the filtered waves, after normalizing. By plotting the normalized envelope as a function of slowness and period, one obtains an estimate of the group velocity of the wave, commonly called a dispersion curve (the colored panel on the right). In this case, the small red dots indicate the maximum power of the envelop as a function of slowness, where the slowness is a function of time and source/station distance.

Chapter 2

Multiwavelets

2.1 Background

Wavelets have been independently introduced in various fields of study since the 1960s (Daubechies, 1992) and first used in geophysics by Morlet *et al.* (1992). In seismology, wavelet techniques have been applied to array processing (Bear and Palvis, 1997, 1999; Bear *et al.*, 1999), spectral estimation (Park *et al.*, 1987), polarization analysis (Lilly and Park, 1995), and seismic gradiometry (Poppeliers, 2010, 2011), among other things. In the context of analyzing surface waves, the wavelet transform is a natural choice for time-frequency decomposition, as it optimizes the trade-off between time and frequency resolution. Furthermore, the wavelet transform provides virtually the same information as the more conventional filter-bank method for analyzing surface waves (e.g. Dziewonski *et al.*, 1969). To see this, consider using a series of narrow-band filters on a seismogram $s(t)$ to isolate the signal's frequency-dependent components:

$$\widehat{S}(t,f_c) = \int_{-\infty}^{\infty} H(t,f_c \pm \Delta f) s(t-\tau) d\tau, \tag{2.1}$$

where t is time and $H(t,f_c \pm \Delta f)$ is a filter with center frequency f_c and a bandwidth of $\pm\Delta f$. Applying equation 2.1 results in a series of band-limited seismograms, $\widehat{S}(t,f_c)$ each with frequency range of $f_c \pm \Delta f$. To highlight the group velocity of dispersive surface waves, the envelope of each filtered and normalized seismogram of $\widehat{S}(t,f_c)$ is taken and plotted as a function of center frequency. Given the starting time of the seismic source and the distance between the source and the observation point, the group velocity of a particular frequency-limited surface wave can be estimated (Figure 1).

The wavelet transform of a signal is given as

$$W[s(u,C)] = \int_{-\infty}^{\infty} \Phi(u,C) s(t-u) du \tag{2.2}$$

where Φ is a real- or complex-valued wavelet function with scale length C and position u. The scale C relates to center frequency and the position u relates to time. To apply Equation 2.2 a wavelet function with scale C is simply convolved with the signal. By re-applying equation 2.2

for a range of wavelet scales, a series of narrow-band decomposition of signal $s(t)$ is produced. The similarity of the wavelet transform to the filter bank shown in equation 2.1 is apparent: the band-limited wavelet functions $\Phi(u,C)$ act as narrow band filters. Figure 2.2 a direct comparison between the two methods: a conventional filter bank versus a wavelet transform. The filter bank method was implemented using a Gaussian filter and the wavelet transform used the first Slepian wavelet (see below for a description of Slepian wavelets). Note that for both cases the transforms were normalized and enveloped for the display.

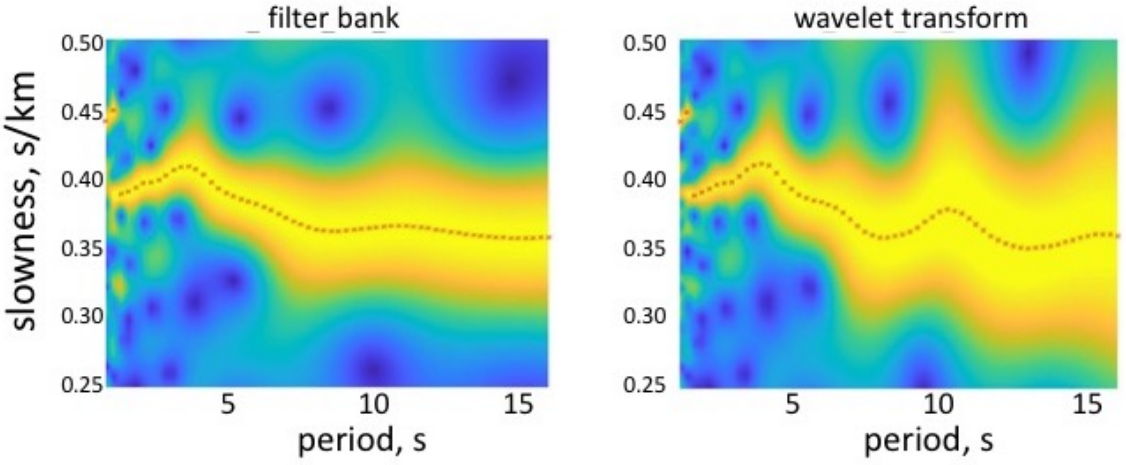

Figure 2.1. The similarity between a conventional filter bank method of decomposing a dispersive seismogram and the multi-wavelet transform. The panel on the left shows the result of a Gaussian filter bank method to estimate the dispersion curve for a cross correlelogram between stations GMN and GWY of the University of Nevada Seismic Network. The right panel shows the result of decomposing the same cross correlogram with a wavelet transform. In both panels, after the signal was decomposed into its constituent time-frequency coefficients, the signal was enveloped and normalized. The small red crosses identify the maximum amplitude of a given slowness-period location, and corresponds to the resolved dispersion curve.

The wavelet function $\Phi(u,C)$ can be of any functional form, so long as it possesses three mathematical criteria:

1. A wavelet must have finite energy:

$$E = \int_{-\infty}^{+\infty} |\Phi(t)|^2 \mathrm{d}t < \infty \tag{2.3}$$

where E is energy.

2. The wavelet must have zero mean. Therefore if the Fourier transform of $\Phi(t)$ is

$$\widehat{\Phi}(f) = \int_{-\infty}^{+\infty} \Phi(t) e^{-i2\pi ft} \mathrm{d}t \tag{2.4}$$

then

$$\widehat{\Phi}(0) = 0. \tag{2.5}$$

3. For complex wavelets, the Fourier transform of $\Phi(t)$ must be real and vanish for negative frequencies.

2.2 Slepian wavelets and the multiwavelet transform

The criteria described by items 2.3-2.5 allow significant freedom in choosing the form of $\Phi(t)$. Although each specific type of wavelet will give slightly different results, they all will produce approximately similar time-frequency decompositions (which is not at all alarming: a similar phenomenon occurs for the filter bank method, depending on the form and bandwidth of the filter used). These differences can be explained by the complex spectrum of the given wavelet type. Regardless, for the work here, I use Slepian wavelets, which are a family of mutually orthogonal, real-valued, even-odd functions that are time-frequency optimized (Slepian, 1983; Thompson, 1982). For a given scale, the suite of wavelet pairs have the same center frequency and bandwidth as all the other wavelet pairs (e.g. figure 1 of Bear and Pavlis, 1997), although each wavelet pair emphasizes a different portion of the spectrum within a given frequency range. Because each wavelet pair is orthogonal to all other wavelet pairs, constructing a series of wavelet decompositions of a signal will result in statistically independent measurements of a signal's time-frequency structure (Bear and Pavlis, 1997; see Figure 2.2 of this report).

Lilly and Park (1995) developed a method of constructing Slepian wavelets to be used for the multiwavelet transform. The wavelets are real-valued, discrete time series Φ_m with M samples and sampling rate of Δt. The wavelet pairs are designed to concentrate energy within a given frequency band f_c and bandwidth $2f_w$, where $f_w \leq f_c$.

Slepian wavelets real valued and thus the energy in the frequency domain appears in both the positive and negative frequencies. Therefore, any frequency band of interest is defined by $|f \pm f_c| \leq f_w$. The fraction of the total energy contained within this frequency interval is

$$\lambda = \frac{\displaystyle\int_{-(f_c+f_w)}^{+(f_c+f_w)} |W(f)|^2 \mathrm{d}f - \int_{-(f_c-f_w)}^{+(f_c-f_w)} |W(f)|^2 \mathrm{d}f}{\displaystyle\int_{-(1/2\Delta t)}^{+(1/2\Delta t)} |W(f)|^2 \mathrm{d}f} \tag{2.6}$$

where

$$W(f) = \Delta t \sum_{m=-P+1}^{R} w_m e^{-\mathrm{i}2\pi f m \Delta t} \tag{2.7}$$

is the discrete Fourier transform of the wavelet w_m of length M, P is the closest integer $\geq M/2$, R is the closet integer $\leq M/2$, and $\mathrm{i} = \sqrt{-1} \neq i$. They are calculated by solving the eigenvalue problem

$$\mathbf{A}\underline{\Phi} = -\lambda\underline{\Phi} \tag{2.8}$$

where

$$A_{mn} = \frac{\sin[2\pi(f_c + f_w)\Delta t(m-n)]}{\pi(m-n)} - \frac{\sin[2\pi(f_c - f_w)\Delta t(m-n)]}{\pi(m-n)} \tag{2.9}$$

and solving for $\underline{\Phi}$ (Lilly and Park, 1995; Bear and Pavlis, 1997). Solving equation 2.8 yields N orthogonal solutions of eigenvectors $\Phi^{\{k\}}$ and associated eigenvectors λ_k, $k = 1, 2, ...N$. The wavelets are formed by sorting the eigenvalues (and their associated eigenvectors) from greatest to least magnitude and then normalized to unity.

For a given scale, the center frequency of the wavelets are controlled by the parameter time-bandwidth product p, where

$$p = f_w M \Delta t. \tag{2.10}$$

Similarly, the bandwidth is controlled by the parameter time-bandcenter product p_c

$$p_c = f_c M \Delta t. \tag{2.11}$$

In practice, the parameters p and p_c are held fixed and the wavelets' center frequency is varied by changing the scale, or time length, M of the wavelet.

The wavelets $\Phi^{\{k\}}$ occur as even-odd pairs, and the wavelets within a given pair are $\pi/2$ radians out of phase. Therefore, the wavelets in each pair can be combined into a complex function

$$\Phi^{\{k\}}(t, C) = \Phi_e^{\{k\}}(t, C) + \mathrm{i}\Phi_o^{\{k\}}(t, C) \tag{2.12}$$

where C is the scale of the wavelet, $\Phi_e^{\{k\}}(t, C)$ is the k-th even wavelet, and $\Phi_o^{\{k\}}(t)$ is the k-th odd wavelet. Finally, the complex function $\Phi^{\{k\}}(t, C)$ can be used as the integrand of the general

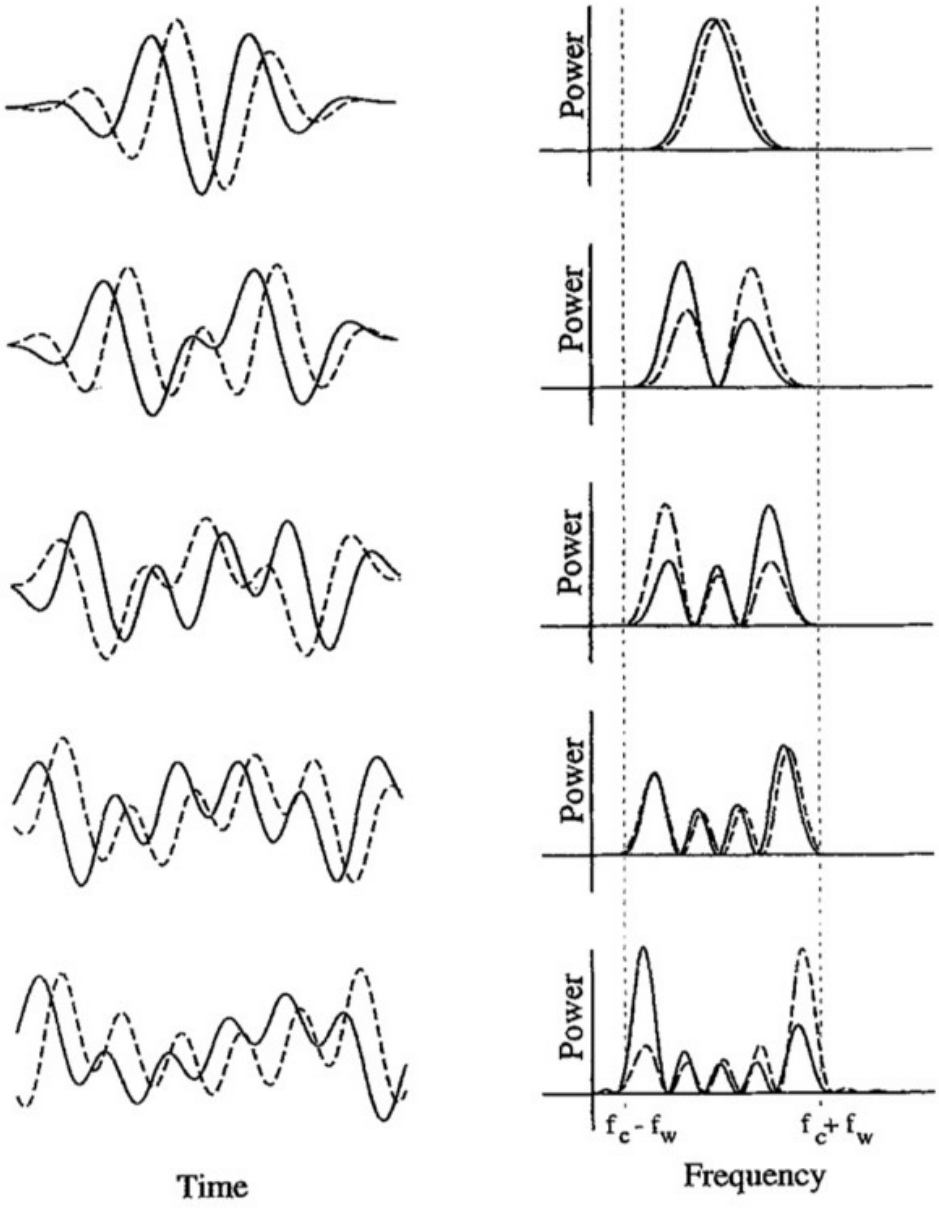

Figure 2.2. Ten Slepian wavelets as calculated from equation 2.8 in time (left panel) and their frequency power spectra (right panel). Figure is from Bear and Pavlis (1997).

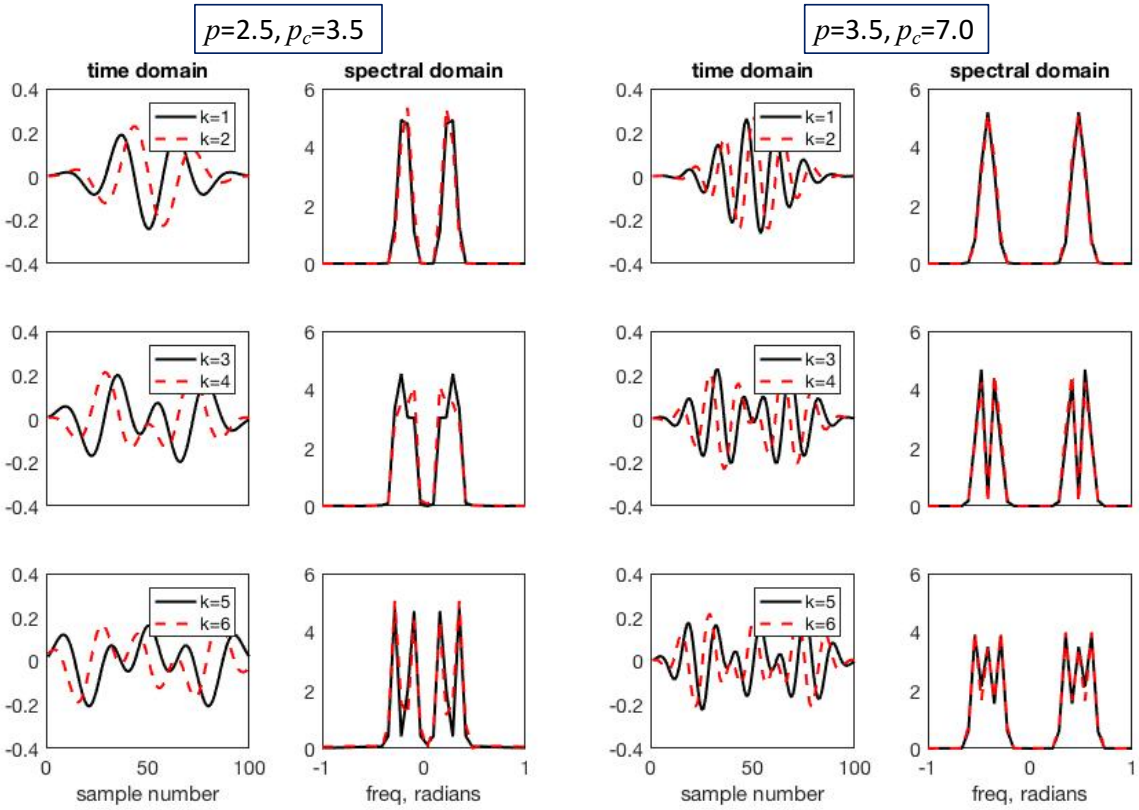

Figure 2.3. An illustration of how the time-bandwidth and time-bandcenter products alter the spectral content of the wavelets. In all the wavelets shown here, the number of samples is identical. In the left half of the figure, the lower values of both p and p_c create wavelets $k = 1, 2, ..., 6$ that have a lower frequency than those in the right half of the figure. Although the center frequency can also be adjusted by appropriately changing the wavelet's scale, note that changing p and/or p_c can also alter which portions of the spectrum are emphasized.

wavelet transform (equation 2.2) to yield the multiwavelet transform:

$$
\begin{aligned}
W^{\{k\}}[s(t,f)] = & \qquad (2.13)\\
= & \int_{t-T/2}^{t+T/2} s(t-\tau)\Phi^{\{k\}}(t,C)\mathrm{d}\tau \\
= & \int_{t-T/2}^{t+T/2} s(t-\tau)\Phi_e^{\{k\}}(t,C)\mathrm{d}\tau + \mathrm{i}\int_{t-T/2}^{t+T/2} s(t-\tau)\Phi_o^{\{k\}}(t,C)\mathrm{d}\tau
\end{aligned}
$$

where there are k complex-valued wavelet transforms of the signal $s(t)$.

There are two important points regarding the use of equation 2.13 for surface wave analysis. First, as argued in equation 2.1, the wavelet, and thus multiwavelet, transform decomposes the data in a similar way as the more conventional filter bank. This allows the user to estimate the group velocity of surface waves as a function of frequency. Secondly, because the k wavelet pairs in equation 2.13 are mutually orthogonal, the resulting transforms are also mutually orthogonal (and thus statistically independent). Therefore, for a population of dispersion estimates corresponding to $k = 1,2,3,...N$ wavelets, standard statistical methods can be employed to obtain estimates of uncertainty. The subsequent uncertainties of group and phase velocities can then be used to place uncertainty bounds on, for example, tomographically estimated subsurface seismic velocities.

Chapter 3

Analysis and Application

To demonstrate the efficacy of the method, I apply the multiwavelet transform to estimate the dispersion curves of selected data sets, and invert the dispersion relations to estimate 1D velocity profiles. My approach is not to present a detailed tomographic analysis of a specific field area but rather to demonstrate the multiwavelet method as applied to 1D surface wave tomography. As such, I first apply the method to a synthetic waveform, where we know what the answer is (in terms of the one-dimensional shear wave velocity profile), and then to two cross-correlograms collected by the University of Nevada Seismic Network.

3.1 General Analysis Procedure

The goal of the analysis is to produce a model of subsurface shear wave velocity with uncertainty estimates. The analysis includes several steps, where judgements must be made at each step regarding processing/analysis parameters. As such, any one step can be repeated as necessary to improve the results, which is fundamentally a subjective judgement of the analyst.

Prior to analysis, it is useful to determine, qualitatively, whether the seismogram is actually dispersive. As such, the focus should be on the low frequency surface wave arrivals. Because the data will be filtered with a sequence of narrow-band filters, I find that the signal-to-noise ratio does not need to be necessarily high, as the filters will eliminate much of the high frequency noise. I find that it's much more important for the analysis that the data actually contain surface wave arrivals rather than having a high SNR. Assuming that the data is appropriate for analysis, the method proceeds as follows (see Figure 3.1 also):

1. Construct a series of analyzing wavelets (equations 2.8-2.12) and convolve them with the data.

2. Take the absolute value of each complex-valued wavelet transform.

3. Normalize each transform and for each period, identify the highest magnitude. The dispersion curve is formed by 'connecting the dots' for each identified slowness-period pair. Each wavelet pair will yield in a dispersion curve.

(a) Note that the multiwavelet transform yields the time-frequency decomposition of a given signal. The time of a given (narrow band) arrival can be used to estimate the slowness if the source-station distance is known: $u = t/d$ where u is slowness, t is the time of the given narrow-band arrival, and d is the station-source distance.

(b) The dispersion curve should 'look smooth'. In other words, the relative change between slowness-period points on a given wavelet transform should be fairly small. In the event that there is a rapid change in the dispersion curve from one point to the next, the offending point(s) should likely be excluded from further analysis.

4. For K wavelet pairs, there will be K dispersion curves. Therefore for each period, there will be a population of slowness estimates. Standard statistical methods can be applied at this point to calculate, for example, the mean and standard deviation of the seismogram at each period analyzed.

5. For my analysis, I compute the mean plus/minus one standard deviation for each period. I use this information to construct three separate dispersion curves: the mean velocity, the low-velocity, and the high-velocity dispersion curves.

   (a) Each dispersion curve is the group velocity for a given seismogram. I also estimate the three corresponding phase velocity curves using the Phase-matched filter method (Appendix 1).

6. For each group/phase velocity curve, I estimate the 1D velocity using the method outlined in Herrmann and Ammon (2004) (sections 3-1 to 3-35) as implemented in their freely available software package Computer Programs in Seismology.

7. The resulting 1D velocity profile computed from each group/phase velocity pair can then be plotted on top of one another, yielding a 1D velocity profile that shows the mean plus-or-minus the uncertainty. In this case, the uncertainty in the 1D shear wave velocity is determined by inverting the low- and high-velocity dispersion curves in bullet number 5.

3.2 Synthetic Tests

The first test is designed to demonstrate the efficacy of the method for a known model. Specifically, I constructed a hypothetical crust/mantle model and numerically propagate an earthquake seismogram through it. The model is constructed to mimic typical crust and mantle seismic properties. We use the freely available software package Specfem3D to model the wave propagation produced by a explosive source located at $[x_0, y_0, z_0] = [150, 0, 0]$km and record the seismogram on a vertical-component station located at $[x, y, z] = [650, 0, 0]$km. The model size is 800 kilometers on a side horizontally, and extends to a depth of 400 km. The resulting vertical component seismogram shows a well-developed dispersion curve (Figure 3.2). We optimized the synthetic seismic source for Rayleigh wave generation by simulating it as a single, downward pointing vector source acting at the surface of the model.

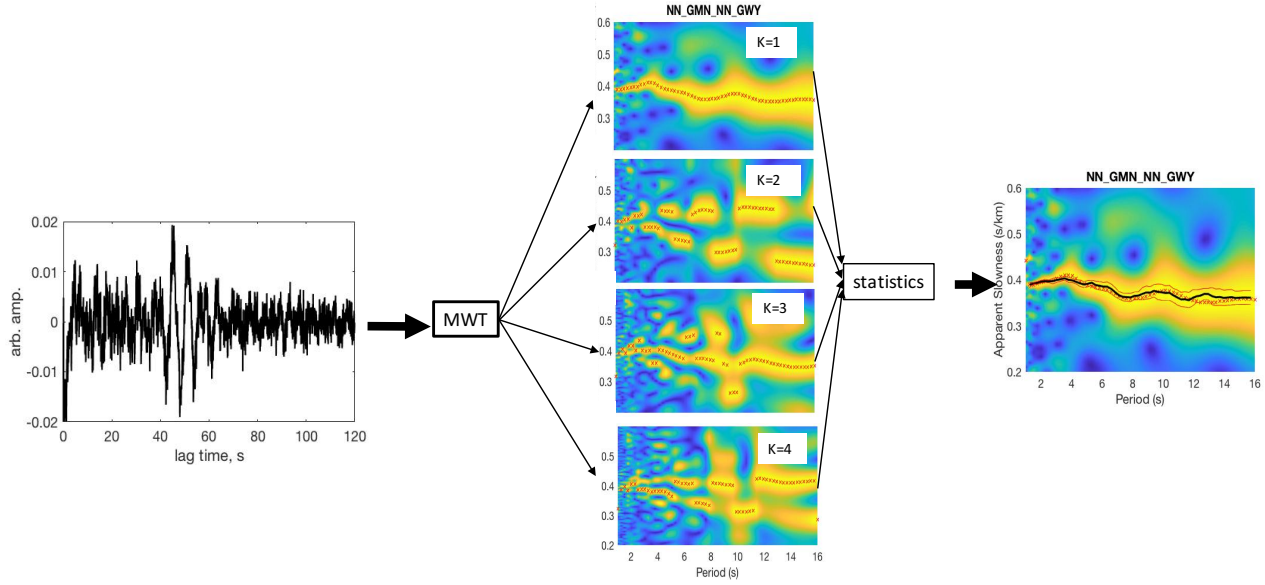

Figure 3.1. An illustration of the steps used to produce a dispersion curve for a single seismogram. The left panel shows the raw cross correlogram collected from stations GMN and GWY of the University of Nevada Seismic Network. In this example, four complex wavelet pairs ($p_c = 3.5, p = 7.0$) are applied to the data. The absolute value of the resulting transforms were then normalized (middle panel), and the maximum power for each frequency is then selected (small red crosses), which form the dispersion curve for that given transform. The group velocity is obtained by knowing the station pair separation and the lag time of the given narrow-band surface wave arrival. The right panel shows the result of using the suite of dispersion curves to compute the mean (heavy black line) and plus-minus one standard deviation (thin black lines). Note that in this example we used ten wavelet pairs to compute the statistics, although only the first four are shown.

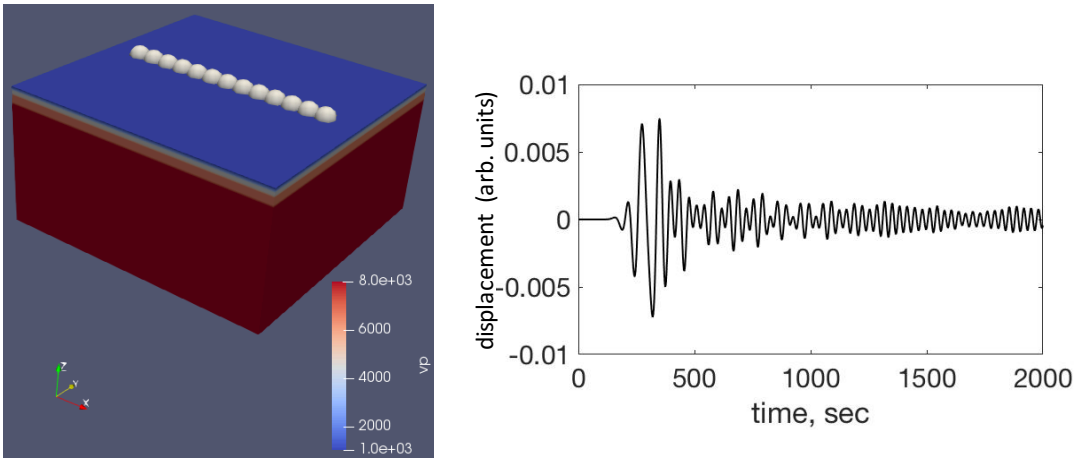

Figure 3.2. The model (left panel) and the resulting seismogram (right panel) computed using Specfem3D. The model is 800km in both horizontal directions, and 400km deep. The color corresponds to the shear wave velocity. The numerical source time function was located at $[x_0, y_0, z_0] = [150, 0, 0]$km and optimized for Rayleigh wave generation, resulting in a (displacement) seismogram that shows clear evidence of surface wave dispersion.

I implement the analysis according to the steps outlined Section 3.1. The bandwidth of the analysis is 35-100 seconds, with sixty evenly space period intervals, where $pc = 7.0$ and $p = 3.5$. To obtain the group velocity, I computed the wavelet transform of the seismogram, and convert the time-period wavelet transform to slowness-period by scaling the time axis to slowness $u = t/d$, where d is the distance between the source and receiver and t is the time. Then for each period in the wavelet transform, I compute power by squaring the magnitude of the complex transform. Note that the resulting transform is similar to computing the envelope of a real function via the Hilbert transform. I then normalize the magnitude transform such that the maximum amplitude for each frequency is one. The maximum envelope amplitude is chosen as the group slowness for that particular period. This procedure is repeated for all of the wavelet transforms. This produces a population of ten estimates of group slowness for each period for the given station pair. I then compute the mean and standard error of the slowness for each period. To compute the phase slowness, I used the phase-matched filter method outlined by Herrin and Goforth (1977).

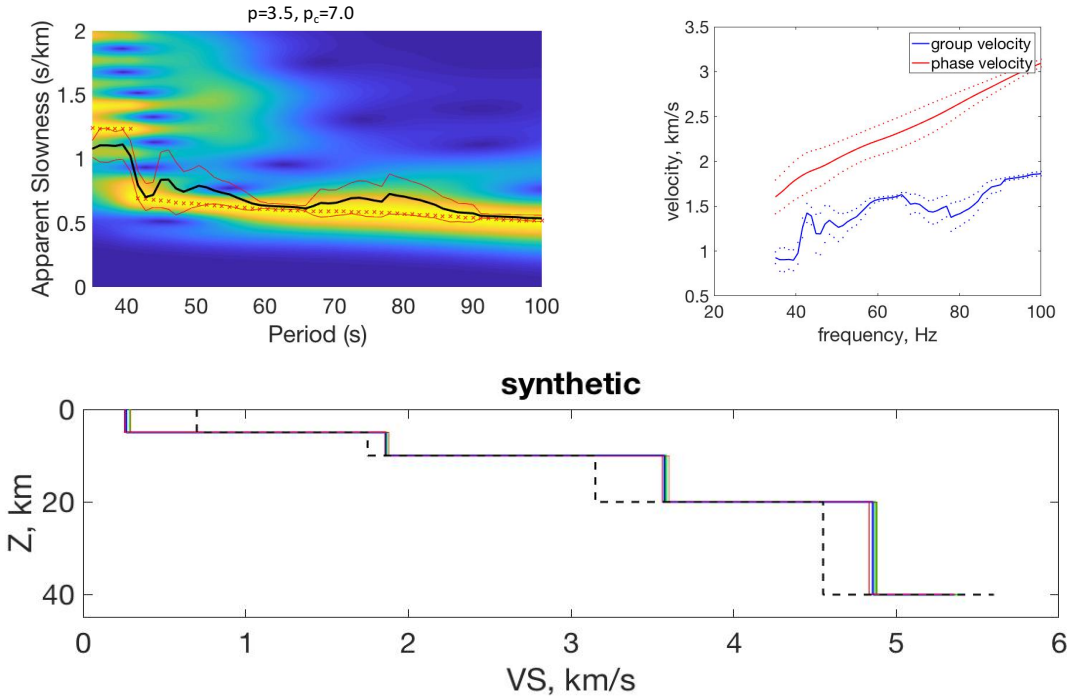

Figure 3.3. Analysis and results using synthetic data. Using the multiwavelet method on the synthetic data (Figure 3.2) resulted in the dispersion curve shown in the upper left hand panel. The resulting group and phase velocities are shown in the upper right hand panel. The results of inverting the group and phase velocities is shown in the bottom panel. See the text for the discussion of the results

.

The results of the multiwavelet analysis of the synthetic seismogram is shown in Figure 3.2.

The observed group velocity curve shows the expected dispersion, however, appears rather variable. Also, we observe that the velocity actually decreases starting at a period of 65s to 80s, which is not an expected result. However, the phase velocity estimates increase monotonically with increasing period. Regardless, the estimated 1D shear wave velocity profile shows increasing velocity with depth. For this test, I used a five layer starting velocity model, which corresponded exactly to the actual model. The inversion underestimated the velocity of the first layer as well as the mantle layer, but over estimated the velocities of the middle, crustal layers. Although the fit doesn't appear good, the point of the analysis was not to perfectly fit the data. Rather, it was to demonstrate that we can propagate the uncertainty in the dispersion curve estimates through the tomographic inversion. Whether the tomographic inversion can fit the data is a topic that is outside the scope of this report.

3.3 Tests with Field Data

To demonstrate the efficacy of the method, I apply it to two high-quality cross-correlograms from the University of Nevada Seismic Network. The cross-correlograms are composed of the station pairs NCF-GWY and AL5S-GWY, and they share a similar ray path. I chose these two station pairs for two reasons. First, they are the highest quality cross-correlograms from this network over the period of 1-16s. Second, the "ray paths" between these station pairs are similar. Stations NCF and AL5S are located approximately ten kilometers apart, and the path from these two stations to GWY is across a sedimentary basin, and a similar distance in both cases (Figure 3.3)

3.3.1 Surface Wave Dispersion Estimates

The data are processed as described in Section 3.1 and the results are shown for both station pairs (Figures 3.3.2 and 3.3.2). For both cross-correlograms, the dispersion curves show a statistically significant (according to the uncertainty) decrease in velocity in the range of approximately seven to ten seconds. This is an atypical behavior for surface wave group velocities, and suggests that there is a prominent low-velocity zone at depth. Although the computed phase velocity relation does not show this decrease in phase velocity with increasing period, its apparent on the estimated dispersion curves.

3.3.2 Surface Wave Tomography

I use the surface wave dispersion curves as well as the uncertainty estimates as input data for 1D surface wave tomography. The inversion algorithm was originally developed by Herrmann and Ammon (2004). To propagate the uncertainty into the tomography inversion, I take the same approach as with the synthetic case: the inversion is performed three times for each dataset: once for the mean dispersion curve and once each for the mean plus/minus the standard deviation. The results of the inversions are shown in Figures 3.3.2 and 3.3.2.

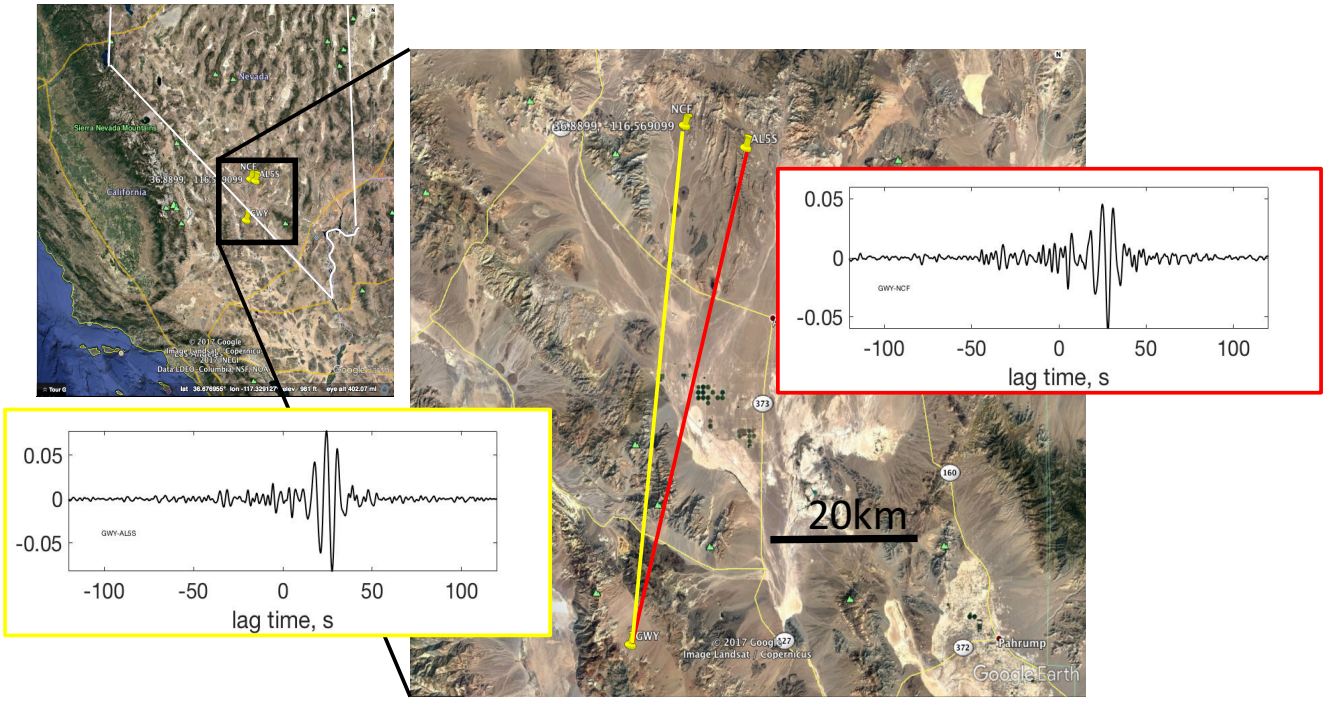

Figure 3.4. A GoogleEarth image of the station pairs used to test the method. The two station pairs (NCF-GWY and AL5S-GWY) are part of the University of Nevada, Reno seismic network. The ray paths of each station pair cross correlogram are shown by the red and yellow line. Note that the color of the outline box on the cross correlograms corresponds to the color of the indicated ray path.

.

The increase in slowness apparent on the dispersion curves occurs for both station pairs over the passband of 7-9 seconds. Regardless of the tomographic results, this fundamental observation implies that there is a low velocity zone in the shallow crust. The rule of thumb is that surface waves are most influenced (in terms of group velocity) at a depth corresponding to approximately 0.6 times their wavelength. If we assume a shear wave speed of upper crustal rocks to be 2.5km/sec, then a Rayleigh with period seven seconds has a wavelength of 17km. Therefore this Rayleigh wave is most sensitive to the the shear wave speed at a depth of 10km. In both of my examples, the low velocity zone is topographically estimated to occur at a depth of approximately 8km. The discrepancy between 8 and 10 km is not terribly significant in 1D surface wave tomography, and when uncertainty is taken into account, the inversion results agree with my "back of the envelope" calculations presented in this paragraph.

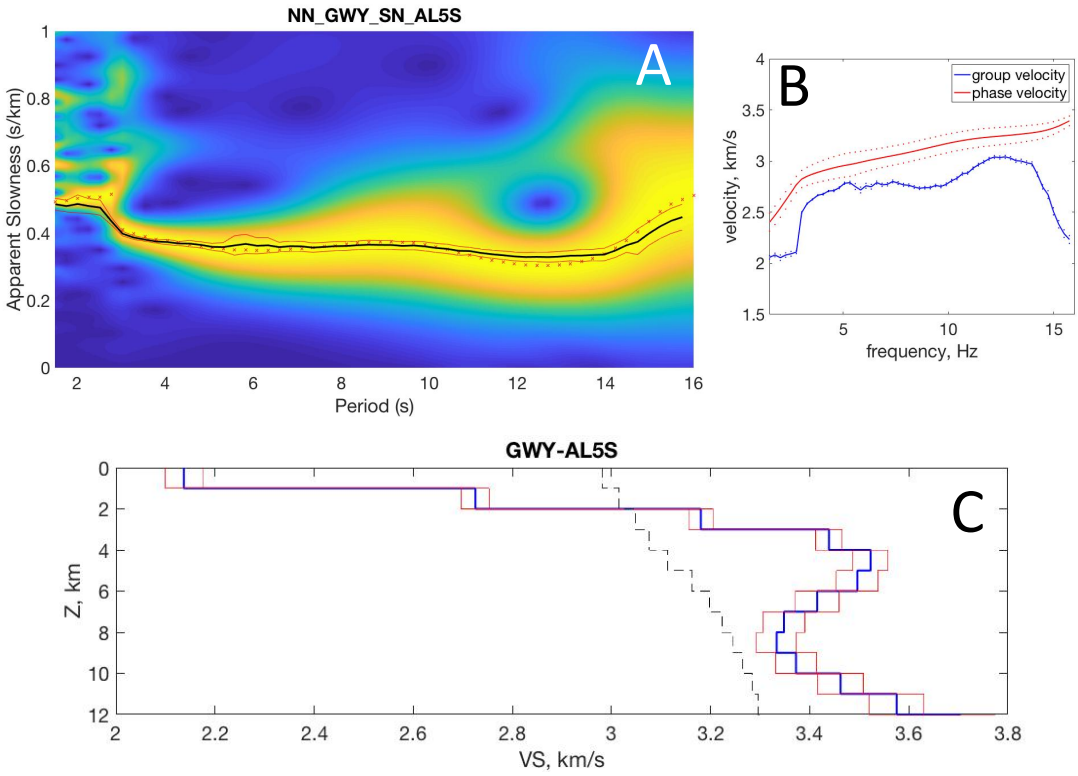

Figure 3.5. Group- and Phase-velocity estimation for station pair GWY - AL5S. The analysis was performed using ten wavelet pairs where p=3.5 and pc=7.0 A) The mean group slowness is shown as a heavy black line where the thin red lines show $\pm$ one standard deviation. The small red crosses show the estimated slowness for the first wavelet pair, which also corresponds to the colormap. B) The group (blue) and phase (red) velocity. The group velocity is simply taken as in inverse slowness from panel A, where the small blue dots correspond to $\pm$ one standard deviation. The phase velocity is estimated using the phase-matched filtering technique that's summarized in the appendix. The uncertainty in the phase velocity is indicated as small red dots. To compute the uncertainty in the phase velocity, the phase-matched filter is computed for each of the three velocity relations: the mean velocity and the mean velocity $\pm$ the standard deviation. C) The results of a 1D surface wave inversion. The inversion used both the group and phase velocity curves shown in panel B. The starting model was composed of twelve layers, each being 1km thick, and is indicated by the black dashed line. The inversion was run three times: once for the mean group and phase, and once each for the mean group and phase velocities $\pm$ one standard deviation. The mean estimated shear wave velocity is shown as the heavy blue line and the uncertainty is indicated by the thin red lines.

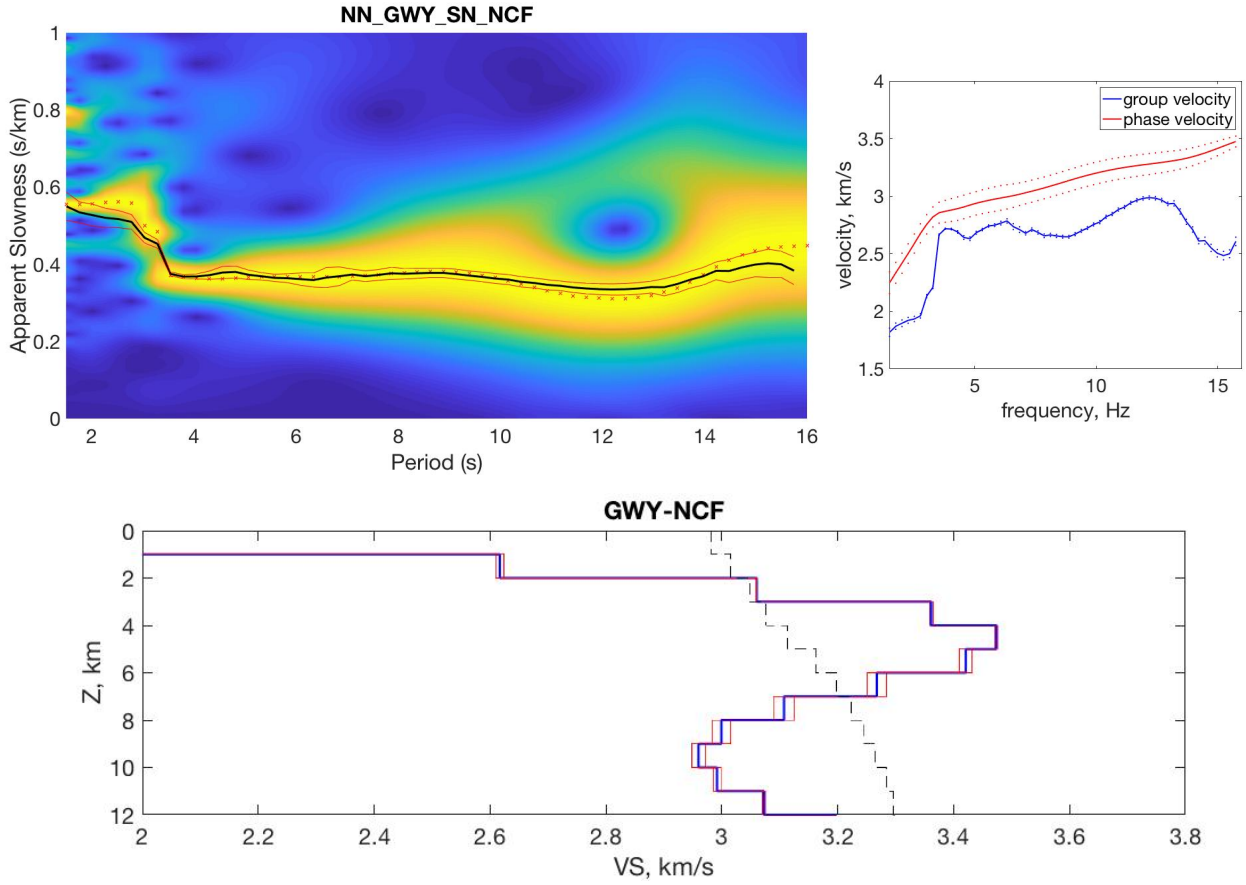

Figure 3.6. Same as Figure 3.3.2 but for station pair GWY-NCF.

.

Chapter 4

Conclusions

In this report, I describe a new single-station method to estimate the dispersion of seismic surface waves. The method is similar to the conventional filter-bank approach in which a series of narrow band filters is used to isolate specific time-frequency portions of the seismogram. I show that the wavelet transform provides a similar decomposition of a seismogram, but one that is optimized in terms of time-frequency tradeoff. By using the multiwavelet transform, I show that the seismogram can be decomposed into a suite of time-frequency estimates, which can be treated as a statistical population. In the case here, I use the multiwavelet transform to decompose the wave field into a series of wavelet coefficients that are localized in time and frequency. Each time-frequency decomposition of the wavefield is used to estimate a statistically independent estimate of the surface wave dispersion curve. Because this method yields a suite of dispersion estimates for a given seismogram, standard statistical methods can be used to estimate uncertainty.

I test the method on synthetic data as well as two cross-correlograms recorded by the University of Nevada Reno seismic network. In each case, I estimate the surface wave dispersion as well as the uncertainty and use this as input into a standard surface wave tomography program. The final result is an estimate of the 1D velocity structure as well as their uncertainties. I did not attempt to perfectly resolve the shear wave velocity structure for either the synthetic case or the two data examples. Rather, I was using 1D surface wave tomography as a demonstration of one possible application, and method, of this type of analysis to estimate Earth structure. I fully recognize the low resolution inherent in 1D surface wave tomography as well as the degree to which it can be "tuned" and/or regularized to favor certain Earth models based on *a-priori* information.

Chapter 5

References

5.1 References

Bear, L. K. and G. L. Pavlis (1997). Estimation of Slowness Vectors and Their Uncertainties Using Multi-Wavelet Seismic Array Processing, *Bull. Seis. Soc. Am.*, **87**(4), 755-769.

Bear, L. K. and G. L. Pavlis (1999). Multi-channel estimate of time residuals from broadband seismic data using multi-wavelets, *Bull. Seis. Soc. Am.*, **89**(3), 681-692.

Bear, L. K., G. L. Pavlis, and G. H. R. Bokelmann (1999). Multi-wavelet analysis of three-component seismic arrays: Application to measure effective anistotropy at Pinon Flats, California, *Bull. Seis. Soc. Am.*, **89**(3), 693-705.

Daubechies, I. (1992). Ten lectures on Wavelets, Society for Industrial and Applied Mathematics, Philadelpia, Pennsylvania.

Dziewonski, A., S. Bloch, and M. Landisman (1969). A Technique for the Analysis of Transient Seismic Signals, *Bull. Seis. Soc. Am.*, **59**(1), 427-444.

Herrin, E., T. Goforth (1977). Phase-Matched Filters: Applications to the Study of Rayleigh Waves, *Bull. Seis. Soc. Am.*, **67**(5), 1259-1275.

Herrmann, R. B., C. J. Ammon (2004). Computer Programs in Seismology: Surface Waves, Receiver Functions, and Crustal Structure, Version 3.30, Dept. of Earth and Atmospheric Sciences, Saint Louis University, accessed at http://www.eas.slu.edu/eqc/eqccps.html.

Lilly, J. M. and J. Park (1995). Multiwavelet spectral and polarization analysis of seismic records, *Geophys. J. Int.*, **122**, 1001-1021.

Morlet, J., G. Arens, E. Fourgeau, and F. L. Vernon (1987). Wave propagation and sampling theory, Part II, Sampling theory and complex waves, *Geophysics*, **47**, 222-236.

Park, J., C. R. Lindberg, and F. L. Vernon (1987). Multitaper spectral analysis of high-frequency seismograms, *J. Geophys. Res., B, Solid Earth Planets* **92**, 12675-12684.

Poppeliers, C. (2010). Seismic wave gradiometry using the wavelet transform: application to

the analysis of complex surface waves recorded at the Glendora Array, Sullivan, Indiana, USA, *Bull. Seis. Soc. Am.*, **100**, 1211-1224, doi 10.1785/0120090304.

Poppeliers, C. (2011). Multiwavelet seismic-wave gradiometry, *Bull. Seis. Soc. Am.*, **101**, 2108-2121, doi 10.1785/0120100226.

Slepian, D. (1983). Some comments on Fourier analysis, uncertainty and modeling, *SIAM Rev.*, **25**, 379-393.

Thompson, D. J. (1982). Spectral estimation and harmonic analysis, *Proc. IEEE*, **70**, 1055-1096.

Appendix A

Phase Match Filter to Estimate Phase Velocity

To obtain an estimate of the phase velocity, I use the method of Herrin and Goforth (1977) assuming group velocities consistent with the PREM continental velocity model. The basic relation is the the (frequency dependent) group delay $t_{gr}(\omega)$ and the Fourier phase angle of the signal are related:

$$t_{gr}(\omega) = \frac{\partial \theta(\omega)}{\partial \omega}, \tag{A.1}$$

where ω is the angular frequency and ω is the Fourier phase. To solve for phase, we separate the variables and integrate:

$$\theta(\omega) = \int_0^{\omega_N} t_{gr}(\omega) d\omega \tag{A.2}$$

where ω_N is the Nyquist frequency. Discretizing equation A.2 yields

$$t_{int}(f_i) = \sum_{i=f_1}^{f_N} t_{gr}(f_i) \Delta f, \tag{A.3}$$

where f_i is discrete frequency and $t_{int}(f_i)$ is related to Fourier phase by

$$\theta(f) = 2\pi(t_{int}(f) - f(t_0) \tag{A.4}$$

where t_0 is the time of the first sample in the seismogram. Note that if the starting time of the seismogram is zero, then $\theta(f) = 2\pi(t_{int}(f))$ which just relates angular frequency to temporal frequency. To obtain the phase velocity, I use the relation

$$c(f) = \frac{\Delta f}{t_{int}(f)}. \tag{A.5}$$

The term $\theta(f)$ can be used to validate the estimated phase velocities by using it to construct a phase-matched filter (PMF). If the phase matched filter $b(f) = S(f)e^{-i\theta(f)}$, where $S(f)$ is the amplitude spectrum of the original seismogram, accurately represents the actual surface wave dispersion along a give source-station path, the cross correlating the PMF with the original seismogram should result in a symmetric, band-limited pulse centered at zero lag at all frequencies (Figure **??**)

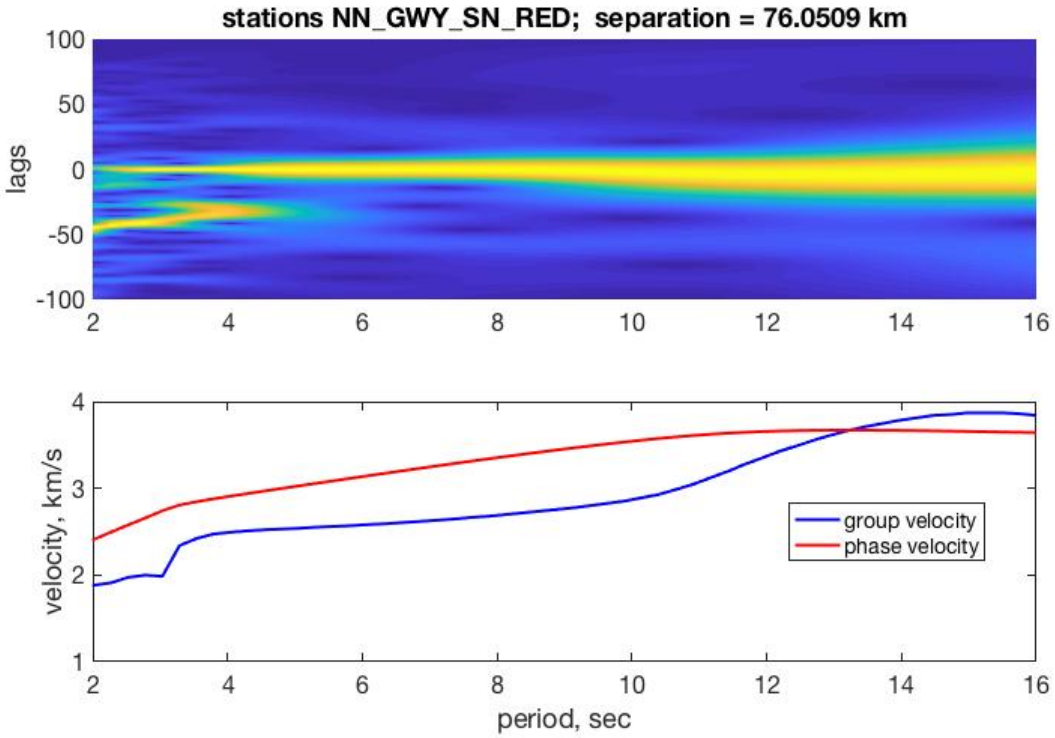

Figure A.1. Applying a phase matched filter to the original correlogram used to construct the group velocity dispersion curve in figure one results in a zero-lag cross correlation at all frequencies. Note that in this case, the PMF does not perfectly remove the dispersion for the smaller periods. The bottom panel shows the group velocities extracted from Figure **??** as well as the estimated phase velocities based on equations A.3-A.5.

DISTRIBUTION:

1	MS 0750	Christian Poppeliers, 8861
1	MS 0750	Leiph Preston, 8861
1	MS 0750	Steven R Vigil, 8861
1	MS 0899	Technical Library, 9536 (electronic copy)


Sandia National Laboratories